Research Article

Insight into the structures of Interleukin-18 systems

Urmi Roy*

Department of Chemistry & Biomolecular Science, Clarkson University, 8 Clarkson Avenue, Potsdam, NY 13699-5820, United States

ARTICLE INFO

ABSTRACT

Structure-based molecular designs play a critical role in the context of next generation drug development. Besides their fundamental scientific aspects, the findings established in this approach have significant implications in the expansions of target-based therapies and vaccines. Interleukin-18 (IL-18), also known as interferon gamma (IFN-γ) inducing factor, is a pro-inflammatory cytokine. The IL-18 binds first to the IL-18α receptor and forms a lower affinity complex. Upon binding with IL-18β a hetero-trimeric complex with higher affinity is formed that initiates the signal transduction process. The present study, including structural and molecular dynamics simulations, takes a close look at the structural stabilities of IL-18 and IL-18 receptor-bound ligand structures as functions of time. The results help to identify the conformational changes of the ligand due to receptor binding, as well as the structural orders of the apo and holo IL-18 protein complexes.

1. Introduction

Immunologically relevant proteins are critical for the functioning of cellular pathways. Therefore, in the general contexts of target-based therapies and drug designs, it is necessary to fully understand how these proteins and their variants participate in the progressions of inflammatory, autoimmune and infectious human diseases (Kabat, 1968; Voit, 2014; Taylor et al., 2017; Gupta et al., 2019; Huang et al., 2019; Jang et al., 2019). The task of gathering detailed knowledge about this topic can be aided to a large extent with residue-level structural analyses of immunologically significant proteins and their interaction with receptors (Moczydlowski, 2013; Xiao et al., 2018; Yao et al., 2019). This investigative approach assists in the proper identifications of therapeutic-targets, their structural-assemblies and consistent ligand-receptor interfacial interactions, and thus, plays a vital role in the development of new, innovative medicines (Freudenberg et al., 2002; Asbury et al., 2010; Haydarlou et al., 2016; Mariethoz et al., 2016; Janwa et al., 2019). The present study of molecular dynamics (MD) simulation (Ho and Hamelberg, 2018; Jin et al., 2020; Weako et al., 2020), focusing on Interleukin-18 (IL-18), falls in this category of computational structural immunology. The main goal of this study is to explore the essential structural and conformational aspects of IL-18 ligand and ligand bound receptor systems.

IL-18, also known as interferon gamma (IFN-γ) inducing factor, is a pro-inflammatory cytokine. IL-18 induces T helper (T_H) cells 1 and 2 responses, and IL-18 signal transduction cascade can also activate nuclear factor kappa beta (NFκβ) (Mak and Saunders, 2006). IL-18, a member of interleukin-1 (IL-1) family, is similar to interleukin-12 (IL-12), and is important for supporting the host defense (Dinarello, 1999; Gracie et al., 2003). IL-18 bridges the gap between innate and adaptive immune responses and is responsible for various inflammatory, autoimmune and physiological conditions, such as inflammatory bowel disease, psoriasis, sepsis, myocardial infarction, Crohn's disease, arthritis and cancer. The IL-18 first binds to the IL-18α receptor (IL-18Rα) and forms a lower affinity complex. Upon binding with IL-18β receptor (IL-18Rβ a hetero-trimeric complex with higher affinity is formed, which initiates the signal transduction process and, triggers the NF-κβ, leading to a downstream transcription through mitogen-activated protein kinase (MAPK) signaling cascades (Kato et al., 2003; Ohnishi et al., 2012; Tsutsumi et al., 2014). As reported by previous authors, IL-1Rrp, the main IL-18Rα, binds to IL-18, but not to IL-1β (Nakamura et al., 2000). Kato et al. have described the first solution structure of IL-18 ligand (Kato et al., 2003). This apo version of IL-18 is further modified by Tsutsumi et al. (Tsutsumi et al., 2014). The ligand bound holo forms of IL-18/IL-18R are also elucidated by Tsutsumi et al. The IL-18 binding protein (IL-18BP) is a cell surface receptor that binds to IL-18 and eventually leads to IL-18 neutralization (Dinarello et al., 2013). A recent study by Krumm et al. has identified the conserved IL-18BP interfacial binding-region on human IL-18 (Krumm et al., 2008).

In recent years, inhibitor based therapies have shown great potentials for further developments in the pharma and biotech sectors (Vogt and Hofmann, 2012; Boulaki et al., 2013; Zamiri et al., 2014; Gonzalez et al., 2015; Lin et al., 2017; Kwak et al., 2018). The treatments of IL-18 related diseases may involve the use of selective or potent IL-18

---

* Corresponding author.
  E-mail address: urmi@clarkson.edu.

ligand-/receptor inhibitors that would interfere with, or effectively block the targeted functions (Hamasaki et al., 2005; Tsutsumi et al., 2019). In our earlier papers we have described the structures and structure-related functional changes of several physiologically relevant proteins (Roy and Luck, 2007; Roy, 2016a, 2016b, 2017, 2019a, 2019b, 2020). The present simulation study examines the structural stabilities of the ligand-protein, IL-18 and IL-18 receptor (IL-18R) bound ligand structures as functions of time. We analyze here the conformational changes within the ligand-protein, due to receptor binding and, we also identify the possible structurally ordered and disordered region within the apo and holo (ligand-bound) protein complexes.

2. Materials and methods

2.1. Protein model selection based on experimental structure

All protein structures were collected from the Protein Databank (PDB) website (Berman et al., 2000) in the form of standard PDB files. For structural studies, we have used Nuclear Magnetic Resonance (NMR) and X-ray crystallographic structures of the human IL-18 ligand-protein 1J0S.PDB (Kato et al., 2003) and 3WO2.PDB, (Tsutsumi et al., 2014). Additionally 3WO3.PDB and 3WO4.PDB, the X-ray crystallographic structures of IL-18α receptor bound IL-18 and the ternary signaling complex of IL-18 have been utilized (Tsutsumi et al., 2014). The 3F62.PDB, an IL-18 complex with IL-18BP of *Ectromelia virus* has also been briefly mentioned (Krumm et al., 2008). The resolution values for the X-ray structures 3WO2, 3WO3, 3WO4 and 3F62 are 2.33 Å, 3.10 Å, 3.10 Å and 2.00 Å respectively.

2.2. Software for simulation and data analyses

Nanoscale Molecular Dynamics (NAMD) and Visual Molecular Dynamics (VMD) programs were used for time-based simulations (Humphrey et al., 1996; Phillips et al., 2005), and the aligned protein sequences were studied with Molecular Evolutionary Genetics Analysis (MEGA 7) (Kumar et al., 2016). IL-18 interactome analyses were performed using the Cytoscope package (Shannon et al., 2003), and 3D protein graphics were developed with Biovia Discovery Studio Visualizer, v16.1.0.15350 (Dassault Systèmes BIOVIA. Discovery Studio Modeling Environment, 2015). The plots were constructed with Origin (OriginLab Corporation, 2016).

2.3. Modeling and simulation

The experimental simulation setup for IL-18 and IL-18/IL-18R were similar to those reported previously (Roy, 2016a, 2016b, 2017, 2019a, 2019b, 2020). Based on the native/original protein, the protein structure file (PSF) along with a corresponding PDB structure was generated. The NAMD software required both the PSF and the modified PDB files as simulation inputs, and these files were created using the Automatic PSF Builder (autoPSF) graphical user interface (gui) of VMD. The topology file, PSF had all the structural information while the modified PDB file contained the predicted hydrogen atoms coordinates. The solvated and neutralized protein structures were obtained using solvate and ionize gui of VMD, where a 0.15 mol/L concentration of NaCl was used for system neutralization.

Energy minimization for the system was performed in 10,000 steps using the NPT ensemble. The final production run was carried out for 20 ns at 298 K using the NVT ensemble and employing the CHARMM force field. A combined version of CHARM22/CHARMM27/CMAP force field was used for this purpose. CHARM22 and CHARMM27 provided the necessary parameter files for the proteins as well as the lipids. The proteins were subjected to phi, psi cross term map (CMAP) corrections (a built-in feature of NAMD plugin gui); these force field parameter files were necessary to calculate the energies. The periodic boundary condition with "Langevin on" control was applied in each case, with an

"active" setting of particle mesh ewald (PME). The Langevin Damping was set to 1. The time steps were set to 1 femtosecond (fs), with 20 steps per cycle selected.

For the basic dynamics, the dielectric value was set to 1.0. The periodic cell basis and periodic cell center were selected according to the PDB coordinates. The time frames of each system were saved as "DCD" files. The output parameters, like DCD/XST output frequency, energy output frequency and restart file frequency, were chosen according to system specifications. Most of these parameters were kept at their default values incorporated in the NAMD gui. This simulation approach is based on the conformational sampling of the predominant (especially early-stage) structural changes of the four systems studied here (Chhatbar et al., 2019; Dimić et al., 2020). The computational protocol was designed to obtain the basic frameworks for the IL-18 ligand and the ligand bound holo structures. Additional computational details of the present work have been described elsewhere (Roy, 2016a, 2016b, 2017, 2019a, 2019b, 2020).

3. Results and discussion

3.1. Analyses of Protein-protein interaction (PPI) network

Fig. 1 illustrates the connectivity of IL-18 within the protein-protein interaction (PPI) network. Table S1 has been included in the Supplementary Data (SD) to list the abbreviations of Fig.1. The PPI is one of the most valuable tools for identifying the ligand-receptor interactions and signaling cascades (Jiang et al., 2015; Wang et al., 2018). The results have been generated by Cytoscape, on the basis of experimental data, as well as manually curated results obtained using the Mentha database (Calderone et al., 2013). Mentha compiles the proteins' key interaction data collected by International Molecular Exchange (IMEx) databases (Orchard et al., 2012) and analyzes the experimental data with a thorough annotation. The interactions considered here are dominated by physical association (as those studied in affinity
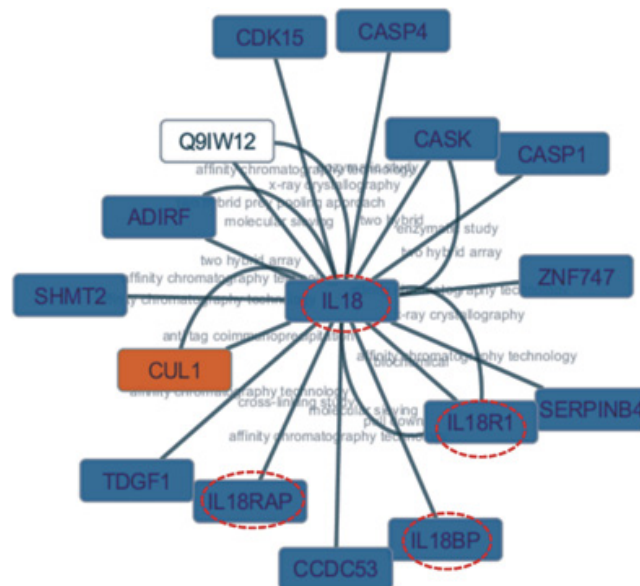

Fig. 1. The protein-protein interactome network of IL-18 is generated using Cytoscape. This PPI network is based on Mentha database, and the primary interaction types are shown in slightly faint text. Within this network, the nodes are the proteins, and the edges denote the latters' shared connections. The node colors correspond to the taxonomic groups; dark blue, orange and white represent *Homo sapiens*, *Mus musculus*, and *Ectromelia virus*, respectively. These are default color codes set up in the software package used to generate the diagrams. The associated abbreviations and other details of the figure are explained in SD table S1.

chromatography, two hybrid array and two hybrid prey pooling), direct interactions (pull down, cross-linking/molecular sieving/X-ray crystallography/enzymatic study and two hybrid), physical interactions (biochemical) and antitag co-immunoprecipitation. The confidence scores are based on a scale of 0–1 where these values reflect the number of functional PPIs curated by experimental procedures as well as based on data from scientific literature. Nonetheless there is always a possibility that a few interactions may be absent. The score between IL-18 and IL-18R1 interaction is 0.539, which is slightly higher than the usual upper bound of a "medium" range. The score near the range of 1 denotes many PPIs as published in scientific literature whereas lower range represents fewer experimental processes. The PPIs identified between IL-18 and IL-18R1 are primarily of physical/biochemical origins. The high affinity signaling complex IL-18/IL-18Rαβ initially activates toll like receptor (TLR) domains, which, via the recruitment of certain adaptor and recruiter molecules, ultimately trigger the NFκβ and MAPK dependent pathways. Binding of IL-18BP to IL-18 leads to neutralization, and the IL-18/IL-18R signaling cascades are no longer induced (Kimura et al., 2008; Krumm et al., 2008; Dinarello et al., 2013).

3.2. Observed protein sequence similarities

The biological sequence alignment between IL-18/IL-1β and IL-18R1/IL-1R type 1 and 2 proteins are plotted in SD Fig. S1 of this report. Fig. S1 indicates notable sequence similarities between IL-18/IL-1β, and also between IL-18R1/IL-1R1 and -1R2. The alignments of IL-18 and IL-18R proteins across the different related species are plotted in Figs. 2–3. Previous authors have noted similar structural and functional similarities between IL-18 and IL-1 and their corresponding receptors (Kato et al., 2003; Yamamoto et al., 2004; Tsutsumi et al., 2014). The alignment schemes presented here (Fig. S1) follow the format used by them. These multiple amino acid sequence alignments are generated using the clustal omega (clustalW) algorithm (Sievers et al., 2011) of MEGA software, (Kumar et al., 2016) along with the incorporation of the Blocks Substitution Matrix (BLOSUM) (Henikoff and Henikoff, 1992). The initial database-search of protein sequence for these analyses was done by Blast. In IL-18 and IL-18R, most of the cysteine (Cys) residues are conserved within different species (Figs. 2–3). Yamamoto et al., have replaced wt IL-18 Cys residues with Serines to make more structurally stable proteins (Yamamoto et al., 2004). In IL-1β, the S-

glutathionylation of a highly conserved Cys residue is considered as a therapeutic target (Zhang et al., 2017). At this time, the possibility of utilizing the conserved IL-18 or IL-18R Cys residues as potential drug targets for various infectious or chronic diseases remains a subject of future investigations.

3.3. Structural information on IL-18 ligand, receptor and ligand-receptor systems

Fig. 4 describes the structures of the ligand IL-18, the IL-18 bound IL-18R proteins, and the IL-18 complex with IL-18BP. Among the 20 conformers submitted to Protein Databank (PDB) we chose the conformer 1 (Model 1) of 1J0S.PDB. 1J0S is a solution NMR structure of IL-18 ligand-protein (Kato et al., 2003). This is a single subunit protein that mostly contains β sheets. The undefined loop structure in 1J0S consists of residues 34 − 42. Fig. 4A displays the secondary structure of 1J0S where the indeterminate loop is identified. Three active sites (I, II and III) are generally considered as the main interacting sites for IL-18Rα (sites I and II) and -18Rβ (site III) receptor chains. Site I is made of five residues Arg13, Asp17, Met33, Asp35 and Asp132. Site II is formed by six residues namely, Lys4, Leu5, Lys8, Arg58, Met60 and Arg104. Site III primarily consists of Lys79, Lys84 and Asp98. The Site III residues are primarily responsible for triggering the cell signaling process (Kato et al., 2003). These residues have been highlighted in a "green stick" mode within the primary interactions site of IL-18 and the IL-18 bound receptor structures.

3WO2 is the X ray crystal structure of wildtype (wt) IL-18 ligand-protein (Tsutsumi et al., 2014). Here the IL-18Rβ binding site (IL-18 site III) is somewhat different from the previously identified region III of 1J0S. Fig. 4B presents the line diagram of 3WO2 where the site III residues (108–110, 112, 145, 147 and 150) are highlighted in the green stick mode. The variable loop region, which is quite prominent in 1J0S, partially turns into α-helical conformation in 3WO2, and has been shown in a different color, grey in Fig. 4B.

Fig. 4C illustrates 3WO3, the X-ray crystallographic structures of the IL-18α receptor bound IL-18 (Tsutsumi et al., 2014). Here subunits A and B represent the IL-18 ligand and the IL-18α receptor, respectively. The α receptor consists of three domains, D1, D2 and D3, where the last two are connected by a relatively longer linker region. The ligand-protein, IL-18 resides within the pocket region formed by these three domains. The ligand-receptor interfacial residues in 3WO3 are
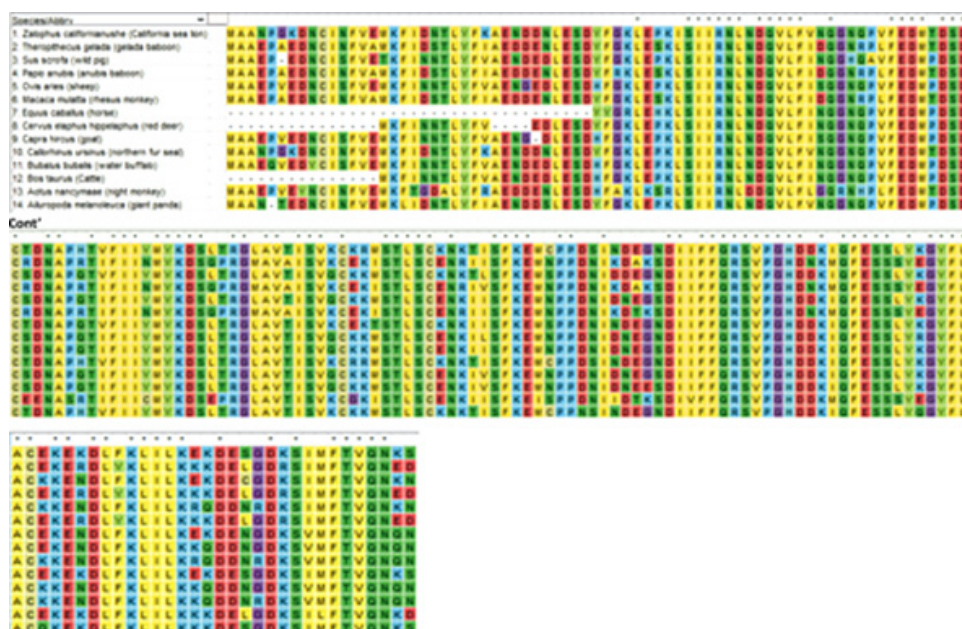

Fig. 2. Alignments of IL-18 protein sequences across different species. These multiple sequence alignments are generated using the clustal omega algorithm through MEGA. The asterix (*) denotes "consensus" throughout the sequences, and the hyphen (-) indicates "sequence gap". The default color codes for specific amino acid residues used in the MEGA software package are displayed, and tabulated in SD Table S2.

Fig. 3. Multiple sequence alignments of IL-18R proteins across different species. The details are explained in Fig. 2 and Table S2.
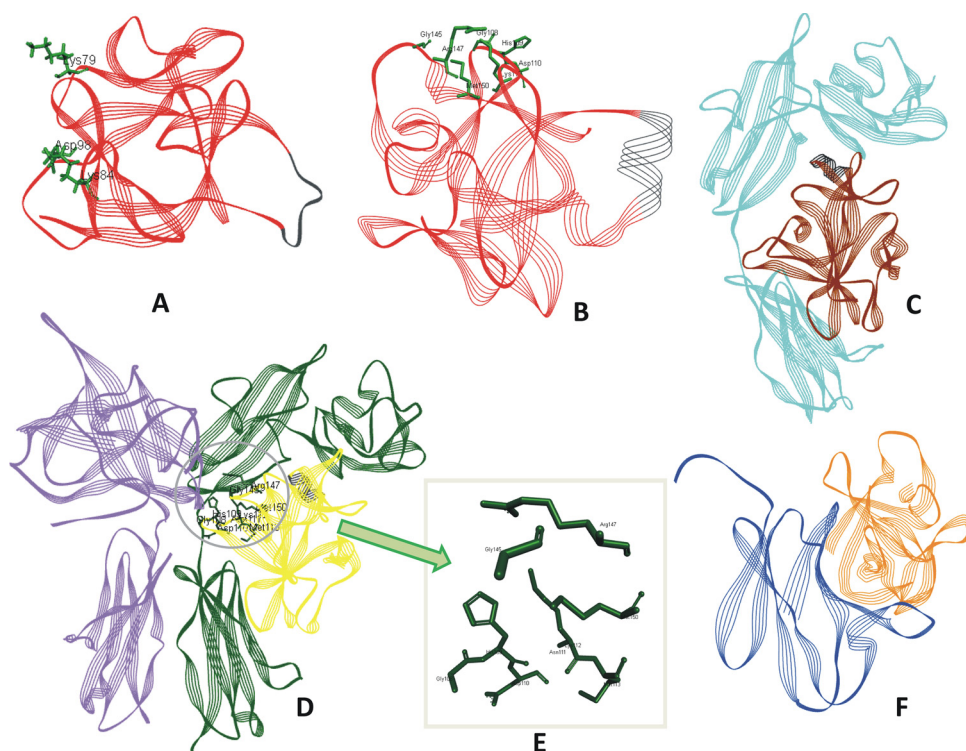

Fig. 4. A Line diagram of 1J0S.PDB where the residues of site III are identified and displayed in green stick mode. The loop region residues (34-42) are depicted in grey. B Secondary structure of 3WO2.PDB where the site III residues are identified. C-D Secondary structures of 3WO3.PDB and 3WO4.PDB, the site III residues of 3WO4 are displayed in the green stick mode. These residues are highlighted in the SD table S4. In B, C and D, part of the loop region, (residues 35-40) that turned into a helical structure has been shown in a different color, grey. E. Closer view of site III residues in 3WO4 ligand. F. Secondary structure of 3F62.PDB. To highlight the main interacting residues, the secondary structures in Fig. 4 have been presented in the line diagrams.

tabulated in SD Table S3.

The X ray crystal structure of the IL-18 signaling complex, 3WO4, is displayed in Fig. 4D (Tsutsumi et al., 2014). This core signaling complex consists of a ternary structure of IL-18 (subunit A), IL-18Rα (subunit B) and -18Rβ (subunit C), with the ligand residing within the D1-D3 pocket of the receptor subunit α. The clusters in 3WO4, consisting of the interface IL-18 residues 31–37, 51–60 and 131–134, that may interact with IL-18Rα. The clusters of interfacial IL-18 residues that possibly interact with IL-18Rβ binding are: 106–110, 144 − 147. The details of the interfacial residues of 3WO4 are tabulated in SD Table S4. The site III residues in 3WO4 ligand are displayed in Fig. 4D. Fig. 4E has been included as a further illustrative addition to Fig. 4D. These primary site III residues have also been highlighted accordingly in SD Table S4.

3F62, an IL-18 complex with the IL-18 binding protein (IL-18BP) of *Ectromelia virus* is displayed in Fig. 4F. This structure of 3F62 has been described by Krumm et al. (Krumm et al., 2008). Part of the IL-18Rα resembles IL-18BP and thus, the binding of IL-18BP with IL-18 blocks the interactions between IL-18 and IL-18Rα (Krumm et al., 2008). The subunits A and B of 3F62 represent IL-18BP and IL-18, respectively. In SD Table S3-S5 we compare the interfacial residues of IL-18 with both proteins, IL-18Rα and IL-18BP. Interactions of the interfacial IL-18 ligand residues with IL-18Rα (3WO3 and 3WO4) and IL-18BP (3F62) are tabulated in SD Table S6. The presences of certain common interfacial interactions between IL-18/IL-18R and between IL-18/IL-18BP can be noted there.

3.4. Analyses of disulfide connectivity in IL-18 systems

Disulfide bonds contribute to protein folding and their conformational stabilities as well as their general functions (Roy et al., 2006; Chatterjee Debnath et al., 2010; Roy and Luck, 2011). 1J0S and 3WO2 have four Cys residues (38, 68, 76 and 127), while none of them forms disulfide bridges (Yamamoto et al., 2004). Like 3WO2, the A subunits of both 3WO3 and 3WO4 contain four Cys residues in the reduced (-SH) form. IL-18Rα (subunit B) of 3WO3 and 3WO4 contains 10 Cys residues, which, in a combination, form five disulfide bridges between Cys22-Cys41, 43–81, 119–158, 140–185 and 237 − 298. IL-18Rβ (subunit C) of 3WO4 has 11 Cys, among which, four disulfide bridges are formed between Cys46-Cys126, 155–180, 175–221, and 273 − 337. The highest disulfide linkages are observed in -α receptor structure of 3WO3 and 3WO4. The positions of the Cys and their linkages in the IL-18 systems are displayed in Fig. 5. The calculated values of most of these S−S bond lengths in 3WO2 and 3WO4 are clustered between 2.01 Å–2.05 Å where the usual disulfide bond is limited to a value of 2.3 Å. For a better understanding of the configuration, these bridges and their bond lengths are mapped in SD Fig S2 (Guex and Peitsch, 1997).

Buried Cys residues play a leading role in determining the protein's structural stability, since buried Cys residues are usually embedded within a protein's hydrophobic core. Being surrounded by various hydrophobic and aromatic residues they form hydrophobic and other nonbonded interactions and thus make the protein structure more compact and stable. In 3WO3/3WO4, most of the Cys residues and disulfide bridges of IL-18 and IL-18Rα receptor chains are buried, and hence, are subject to the aforesaid stability criterion. In the 3WO4: IL-18Rβ subunit, however, the Cys residues and some of the disulfide bridges are mostly surface-exposed. In our previous paper, we have addressed the Cys residue stability resulting from metal binding or structural effects (Roy and Luck, 2011). Here, our goal is to examine how disulfide connectivity increases the overall stability in a protein complex. Previous authors explored the possibility of mutating Cys (-SH) to increase the overall stability of a protein (Yamamoto et al., 2004).

3.5. Molecular dynamics simulations

To check the overall efficacy of the 3D models, the initial protein structures were assessed. Ramachandran plots for the initial structures used in MD simulation are depicted in SD Fig S3. These plots illustrate the favored, allowed and disfavored distributions of phi (φ)/psi (ψ) dihedral angles. The structural evaluations of these figures ensure that most residues are within the favored and allowed region (Lovell et al., 2003). Overall, these plots indicate the effectiveness of the 3D structures; further details are explained in the SD.

Fig. 6 describes structure based property changes detected during the MD simulations of IL-18 ligand and ligand bound receptor systems. Fig. 6A depicts the time-based stability changes of these four systems along with the loop region stability variations within the apo structures. The stability of a system can be determined by its RMSD variations during the simulation time-frame. Other factors that govern the stability of a protein structure/conformation include the root mean square fluctuation (RMSF), as well as findings based on H bonding analyses and secondary structure variations. A visual observation of plot 6A reveals that the overall RMSD values of 1J0S are higher than those of 3WO2. The calculated average RMSD value of 1J0S is greater (3.16 Å) than 3WO2 (2.47 Å). The first 0.6 ns of the simulation was skipped for averaging as initial sampling indicated a steep rise owing to the process of protein-unfolding. These observations gathered from plot 6A lead us to conclude that, apo ligand 3WO2 is more stable than 1J0S. The undefined loop structure and Cys (-SH) residues in 1J0S make this structure less stable. Four Cys (-SH) residues also exist in 3WO2, where the Cys76 and Cys127 species support sulfur-pi interactions with Tyr120 and Phe134, respectively. These sulfur-pi interactions are absent in 1J0S. Though the Cys127-Phe134 pair involves pi-alkyl interactions in both cases. Although some minor variations are observed in 3WO2 loop, overall it maintains a stable nature. The partial conversion of turns into α-helices in 3WO2 strengthens and stabilizes this structure. The undefined loop region in 1J0S is relatively less stable. Fig. 6A also demonstrate how MD simulation can indirectly measure the conformational flexibility within this distinct sequences shared by the two systems, 1J0S and 3WO2. Generally, the ligand bound binary 3WO3 is more stable than the ternary structure, 3WO4. Although RMSD variations are observable in both ligand bound receptor complexes, the last ~2.5 ns of the simulation remains stable and acquires adequate plateaus, as shown in SD Fig. S4. The sulfur-pi interactions observed between Cys76-Tyr120 in 3WO2, are also present in 3WO3 and 3WO4; however, the interaction between Cys127-Phe134 is absent here, despite the signatures of pi-alkyl interactions observed between Cys127 and Phe30 in all three systems, 3WO2 − 4. The interfacial ligand/receptor residues for all these three protein complexes are listed in SD Tables S3-S5. Later in this report, we will discuss the effect of receptor binding on ligand's conformational and structural stability during the simulation time-scale. An exploratory 10 ns RMSD graph for IL-18/IL-18BP, 3F62 is plotted in SD Fig. S6, and this graph indicates a general temporal stability of the structure.

Fig. 6B represents the stabilities of Cys (-SH) and the cystines within the protein and protein complexes. In the protein 1J0S, the Cys residues show considerable variations. The position of a Cys residue in the variable loop region probably causes this variability. The absence of sulfur-pi interactions, as noted above, may also contribute to structural instability. The Cys in the 3WO2 apo form, however, seem quite stable. The ligand bound binary 3WO3 structure show somewhat elevated RMSD, while the reduced Cys (-SH) in the ligand and cystines in the receptor seems to display an observable degree of stability.

For the ligand bound ternary structure 3WO4, the β receptor exhibit strong RMSD variations compared to those of the ligand and α receptor structures (data not shown). The larger interfacial regions of the α receptor (both with ligand and the β receptor) most likely boost the latter's stability, because the stronger inter-subunit interactions operate in these regions. The existence of three Cys residues in the β receptor
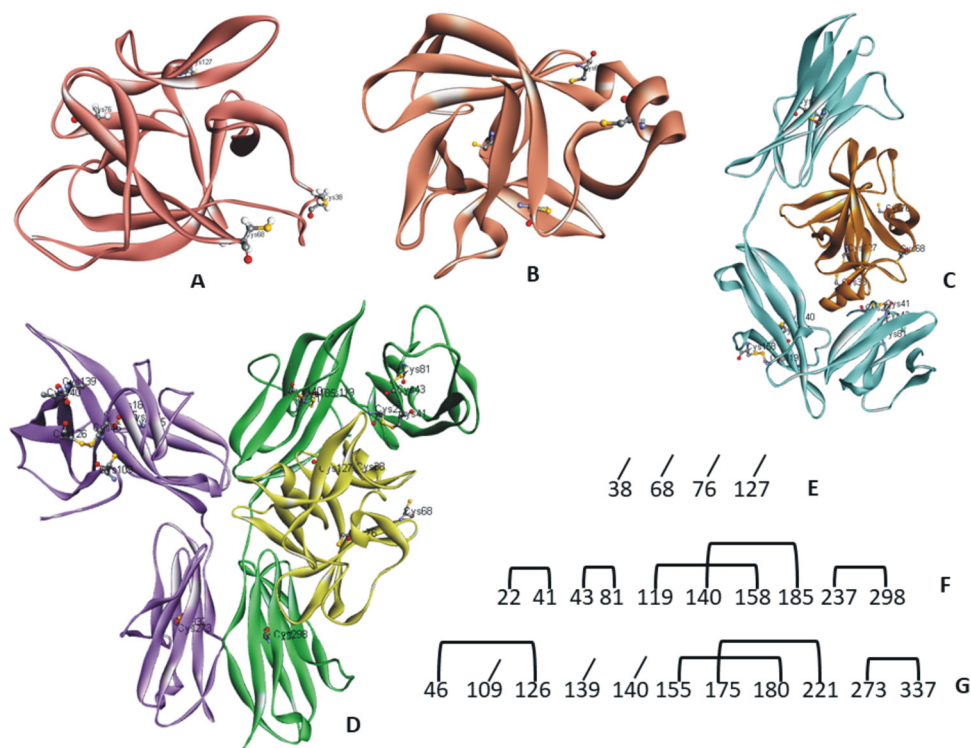
Fig. 5. A-D Cys residues and cystine bridges in A. 1J0S, B. 3WO2, C. 3WO3 and D. 3WO4. E-G Scheme of disulphide connectivity in the IL-18 systems. E. Cys residues of IL-18 ligand in 1J0S, 3WO2, 3WO3 and 3WO4 (subunits A). F. Cystine bridges of IL-18α in 3WO3 and 3WO4 (subunits B). G. Cys residues and cystine bridges of IL-18β in 3WO4 (subunit C). Details of the disulfide mappings are displayed in SD Fig. S2.
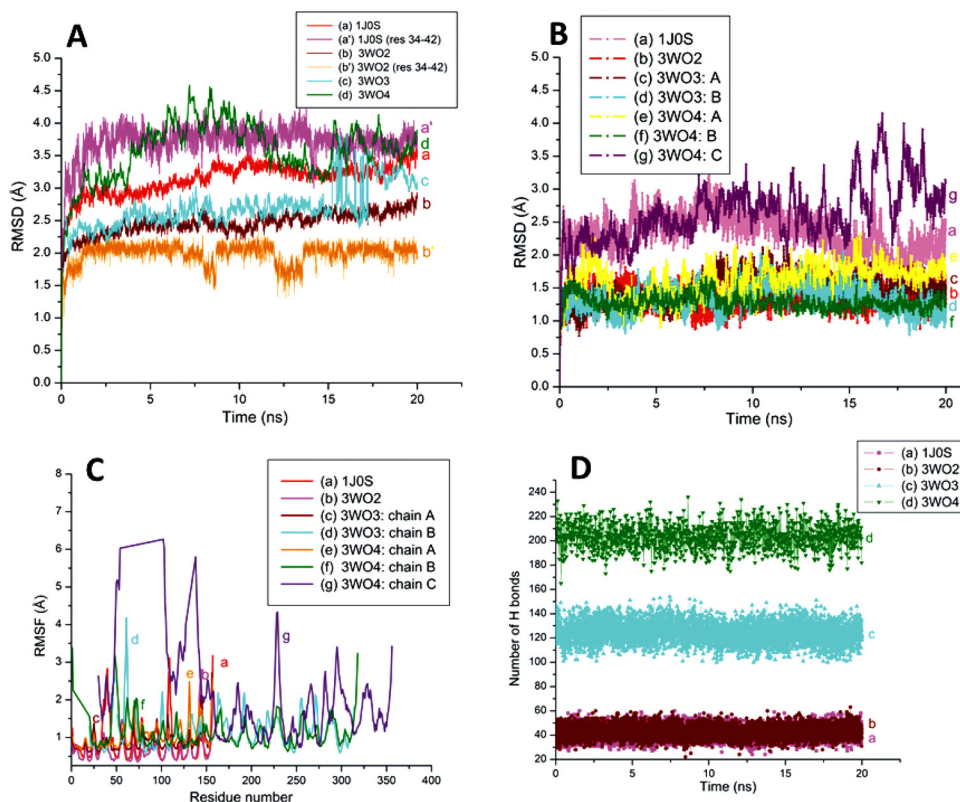

Fig. 6. A RMSD graphs for the apo IL-18 and ligand-bound holo IL-18R systems, with a comparison of the loop regions in apo ligands. B RMSD plots of the Cys residues and cystine bridges in the IL-18 apo and holo systems. C Alpha carbon RMSF plots for the apo IL-18 and IL-18 ligand-bound holo systems. D Time dependent variations in the number of hydrogen bonds for all four systems studied here.

could be attributed to the latter's unstable nature. The presence of surface exposed Cys in the IL-18Rβ receptor chain may also be accountable for the β-chain's higher instability. It is possible that, these fluctuations in the β receptor (Fig. 6B) cause the overall instability of the ligand bound receptor's trimeric structure (Fig. 6A). SD Fig. S5 shows the superposed Cys and the disulfides within the IL-18 systems.

Fig. 6C presents the RMSF plots for the four systems. The X-ray structure of monomeric IL-18 ligand 3WO2 is quite stable throughout the timescale. Among the ligand bound receptor systems, the binary structure is more stable than the ternary ligand-receptor complex. The IL-18Rβ chain of the ligand-receptor complex exhibits significant levels of fluctuations; the underlying causes of this higher fluctuation have been described previously, and could be linked to their elevated RMSD values. The H-bond analyses with time are displayed in Fig. 6D, which
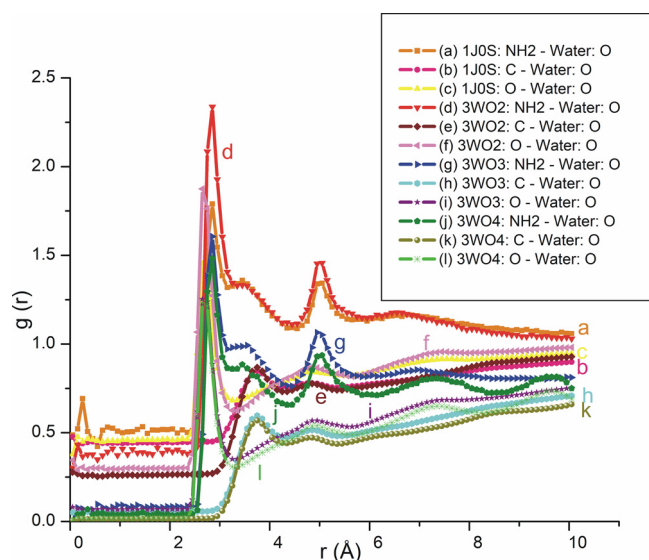
Fig. 7. The radial distribution functions between different molecules of IL-18/ IL-18 ligand bound receptor systems and water. The density, g(r) is plotted as function of radial distance, r (Å).

shows a relatively stable apo-form of 3WO2, and suggests no major temporal changes in the number of the associated hydrogen bonds.

The pair correlation function or radial distribution function (RDF) provides a measure of the atoms' local density, g(r), as a function of the distance (r/Å) between the relevant units considered. RDF values were calculated for protein's amide, carbon and oxygen and water (oxygen) during the simulation time. These calculations led to estimates for the distribution of water-bound oxygens surrounding the proteins' certain atoms or atom groups. Fig. 7 displays these RDF graphs for the four systems, where δr and maximum r were set to 0.1 and 10 Å, respectively. The relatively larger peaks in the RDFs are the indicators of stronger interactions between pairs of atoms, and correspond to comparatively more ordered structures (VanSchouwen et al., 2008). Based on RDF profiles seen in Fig. 7, it is possible to infer that the water oxygens around the proteins' NH_2 group are associated with stronger interactions compared to those of the C or O atoms. The O atoms of the protein are most likely buried to a large extent. The structural ordering of the three interacting groups in these proteins could be written as: $NH_2 > C > O$. From Fig. 7, we can also conclude that, 3WO2 and 3WO4 are the most and least ordered structures of the protein, respectively. The C—O and O—O plots for all four proteins, and in particular, those for the 3WO4 structure show somewhat broader peaks after the first shell. These broad peaks are likely linked to the rather wide range of data-distribution. The somewhat jagged character of the curves with the higher g(r) values of initial distances (r) can be attributed to intrinsic noises/artifacts of the simulation process. The data included in this figure are also presented in a different form in SD Fig. S7, where for additional clarity, the results for the four individual systems are displayed separately.

The time-based graphs in Fig. 8, produced using VMD timeline, display the secondary structural changes of the four systems. To enhance clarity of the detailed elements of this figure, a close-up amplified view of this figure is presented in SD Fig. S8. The secondary structural changes of the ligand and the receptor from the ligand bound receptor systems, 3WO3 and 3WO4 can be separtely viewed in the latter figure. Zoomed-in views of the apo IL-18 ligands, IJ0S and 3WO2 are also shown in Fig. S8. In 1J0S, the loop regions 36–42 and 56–61 show minor secondary structural variations. Moderate to high secondary structure changes are observed in loops 106–111 and 141 − 146. In 3WO2, residues 38–41 remain stable in their helical structure while residues 76–81 continuously change from their 3–10 helical structures

to form turns. Residues 56–60, 96–101 and 106–111 also change from turns to coils.

A change from 3–10 helices to turn is observed around residues 41–44, within the ligand bound form of the 3WO3 ligand. Like the case of 3WO2, in the 3WO3 ligand, the residues around 76–81 also persistently change from 3–10 helical structure to turn. Aside from this, no other major changes are observed in this case, and overall the ligand in 3WO3 seems slightly more stable than that of 3WO2. The receptor residues 256–261 and 282–295 in the linker-turn region of 3WO3 show a few changes from turn to coils and 3–10 helices respectively. Nevertheless, within the receptor structure, the prominent loop region 207–215 seems rather stable. It is likely that, the protein-protein inter-subunit interactions act to stabilize this loop.

From the structure of 3WO3 it is also clear that the IL-18 fits very well within the typical ligand binding pocket by surrounding receptor domains. Certain accommodative arrangements taking place between the ligand and the receptor's three different domains may make the corresponding region further stable.

It is also evident from Fig. 8 that, the ligand is a bit more stable in the receptor bound form of 3WO3, as compared to the corresponding case of the apo structure 3WO2. The secondary structure of 3WO4 ligand has an approximately comparable or marginally higher stability with respect to that of the 3WO3 ligand. However, the 3WO4 ligand residues 66–71 show some additional variability from β-sheets to turns. Nevertheless, the changes that are observed around residue 56 in 3WO3 ligand are absent here. The secondary structural changes of the ligand within the ligand bound receptors are plotted in SD Fig. S8. From Figs. 8 and S8, it is evident that, the ligand is more stable within the receptor-bound forms than in its apo form, and that correspondingly, fewer conformational changes occur within the ligand of 3WO4 upon receptor binding. The IL-18 in 3WO4 is somewhat more stable than 3WO3, even though the overall stability in 3WO3 is higher than that of 3WO4; the relatively higher interfacial inter-subunit interactions present in 3WO4 ligand may be responsible for this higher stability.

The maximum changeability in the secondary structure is observable in the C subunit (IL-18Rβ of 3WO4. The residues around 46–53, 116–119, 200 and 215 of the C chain frequently change from turn to coils or helices. Although one energetically significant cation-pi interaction (Arg147/Tyr212) is present between the subunits A and C of 3WO4 (Gallivan and Dougherty, 1999), the small interfacial overlap between IL-18 and IL-18Rβ (as well as the geometry of the -β chain) could be related to the destabilizing character and the variations within the secondary structure of 3WO4.

Fig. 9 presents the total and non-bonded energy plots (van der Waals and electrostatic energies) in the final stage of the simulation for all the four systems studied. Following standard practice (Laberge and Yonetani, 2008; Průša and Cifra, 2019) this plot has been generated based on the observations made in the final 2.5 ns of the full (20 ns) sampling span. These energy plots provide a general evaluation of the protein/protein complexes' temporal stabilities. The plots show some fluctuations within the ligand bound hetero-dimeric receptor, while they also display an overall steady-state profile within the rest of the structures. According to these data, the monomeric apo-forms are the most stable, and among the holo-structures, 3WO3 remains steadier than 3WO4. While the ligand with receptor dimers has more inter-subunit interactions than those of the ligand-receptor monomer system, the conformational freedom of 3WO3 likely plays a key role in the latter's structural rearrangement; eventually, this results in a relatively stronger and ordered form of this structure.

The interactions between IL-18 ligand and its receptor, along with several adapter molecules, trigger various signaling pathways responsible for immuno-regulatory as well as immunomodulatory activities. We have identified the main ligand/receptor interaction sites in IL-18 systems based on the available PDB structures. Their time-based stabilities are also assessed. Over-reactivity and imbalance of IL-18 can be the causes of various diseases; the ligand-receptor interactions and
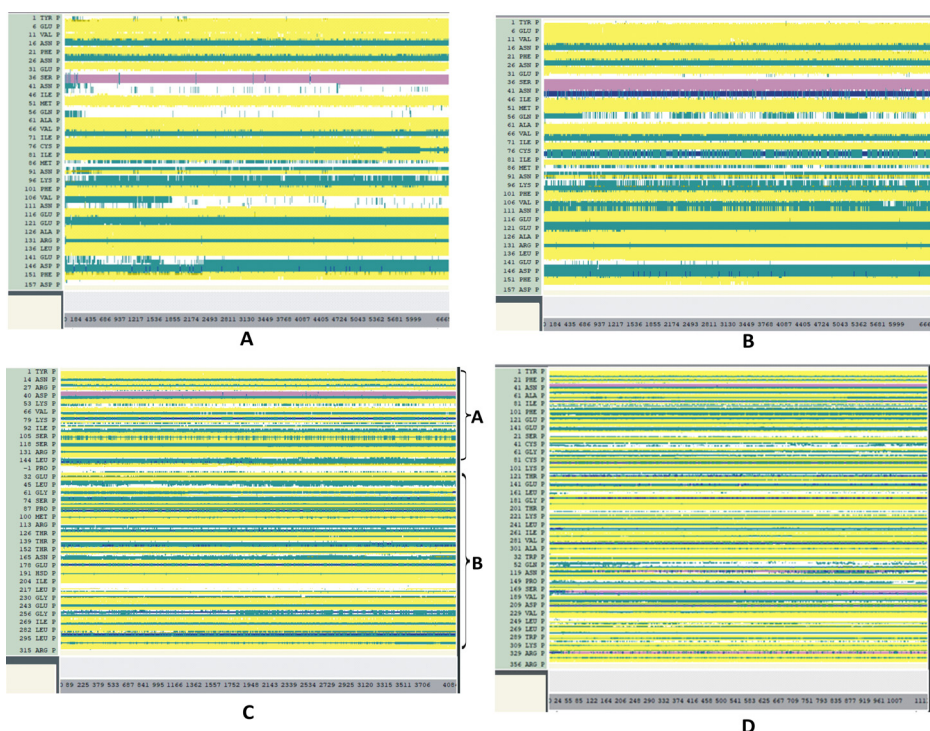
Fig. 8. A-D Time based changes within the secondary structure of: A. 1J0S.PDB; B. 3WO2.PDB; C. 3WO3.PDB (chains A and B) and D. 3WO4.PDB (chains A, B and C). The X-axis indicates the residue numbers and the Y-axis represents the time frames. The zoomed in view of this figure is presented in the SD as Fig. S8. The scheme of the color codes used in this figure is described in SD Fig. S8H.

the interactions between ligand and IL-BP, as those described in this paper, can help to design proper IL-18/IL-18R inhibitors. Additionally, IL-18 plays a major role in infection related inflammation such as coronavirus or influenza virus infections. A recent study reveals that in case of murine coronavirus infection, IL-18 enhances the immunity by releasing IFN-γ (Zalinger et al., 2017).

Furthermore, along with several other cytokines, IL-18 can be used as adjuvants with HIV and several other vaccines (Bradney et al., 2002). In recent years, due to outbreak of SARS-CoV-2 pandemic, considerable attentions have been directed towards the immunity development against viral pathogens. The present paper demonstrates that, IL-18 itself is a structurally steady protein and that it can retain this stability over a relatively extended time-scale. This observation points at the potential use of IL-18 as an adjuvant for antibody generation and

immune enhancement, which, in turn could facilitate future strategies to develop novel treatments for communicable viral diseases.

4. Conclusions

The computational results presented in this work describe a set of residue-level analyses of the IL-18 systems based on their published structures. This investigation also explores the PPIs between the IL-18/IL-18R and the IL-18/IL-18BP systems, and notes the relevance of the findings. The time-based structural stabilities of IL-18, in both its apo and ligand bound holo forms have been measured using MD simulation. The results show that, the ligand is somewhat more stable in its receptor bound structures. The ligand bound receptor monomer 3WO3 has been found to be somewhat more stable than the ligand bound receptor
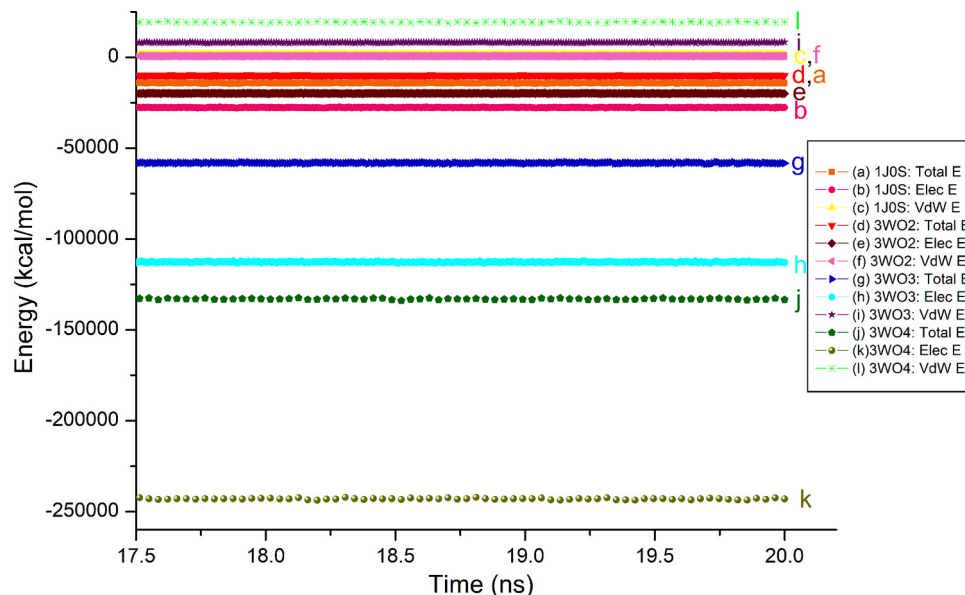

Fig. 9. Time based energy profiles of the four IL-18 systems examined, showing the final 2.5 ns of the simulation run.

dimer 3WO4. The immunological significance of IL-18 signaling is rooted in the fact that, IL-18 is related to numerous autoimmune and inflammatory diseases, and that the interruption of IL-18/IL-18R signaling cascades impact the development of anti-inflammatory drugs/drug-targets. Additionally, IL-18 upregulates Fas ligand and interferon gamma (IFN-γ) leading to the process of apoptosis or cell death. IL-18 biologics may be relevant also in the contexts of immunity enhancement approaches. Thus the detailed identification of the ligand/receptor interfaces of this protein, and subsequent identification of targeted-therapy based on computer modeling efforts, as those discussed in this paper, could be helpful in the development of predictive immunotherapy and precision bio-therapeutics.

Author statement

The author has attached all high resolution figures (Figs. 1 to 9 and graphical abstract) as Zip files.

Declaration of Competing Interest

The author declares no conflict of interest.

Appendix A. Supplementary data

Supplementary material related to this article can be found, in the online version, at doi:https://doi.org/10.1016/j.compbiolchem.2020.107353.

References

Asbury, T.M., Mitman, M., Tang, J., Zheng, W.J., 2010. Genome3D: a viewer-model framework for integrating and visualizing multi-scale epigenomic information within a three-dimensional genome. BMC Bioinformatics 11, 444.

Berman, H.M., Westbrook, J., Feng, Z., Gilliland, G., Bhat, T.N., Weissig, H., Shindyalov, I.N., Bourne, P.E., 2000. The protein data bank. Nucleic Acids Res. 28, 235–242.

Boulaki, V., Vlachakis, D., Sotiraki, S., Kossida, S., 2013. An up-to-date review of piglet isosporosis: new insights and therapeutic perspectives. Int. J. Syst. Biol. Biomed. Tech. 2, 49–62.

Bradney, C.P., Sempowski, G.D., Liao, H.-X., Haynes, B.F., Staats, H.F., 2002. Cytokines as adjuvants for the induction of anti-human immunodeficiency virus peptide immunoglobulin G (IgG) and IgA antibodies in serum and mucosal secretions after nasal immunization. J. Virol. 76, 517–524.

Calderone, A., Castagnoli, L., Cesareni, G., 2013. Mentha: a resource for browsing integrated protein-interaction networks. Nat. Methods 10, 690–691.

Chatterjee Debnath, M., Roy, U., Krishna Halder, K., Sarkar, B., Sinha, S., Ganguly, S., 2010. Technetium-99m cysteine; a novel radiopharmaceutical for detection of experimental myocardial infarction in rats. Curr. Radiopharm. 3, 290–296.

Chhatbar, D.M., Chaube, U.J., Vyas, V.K., Bhatt, H.G., 2019. CoMFA, CoMSIA, Topomer CoMFA, HQSAR, molecular docking and molecular dynamics simulations study of triazine morpholino derivatives as mTOR inhibitors for the treatment of breast cancer. Comput. Biol. Chem. 80, 351–363.

Dassault Systèmes BIOVIA. Discovery studio modeling environment. San Diego 2015.

Dimić, D., Milanović, Ž., Jovanović, G., Sretenović, D., Milenković, D., Marković, Z., Dimitrić Marković, J., 2020. Comparative antiradical activity and molecular Docking/Dynamics analysis of octopamine and norepinephrine: the role of OH groups. Comput. Biol. Chem. 84, 107170.

Dinarello, C.A., 1999. Interleukin-18. Methods 19, 121–132.

Dinarello, C., Novick, D., Kim, S., Kaplanski, G., 2013. Interleukin-18 and IL-18 binding protein. Front. Immunol. 4.

Freudenberg, J., Zimmer, R., Hanisch, D., Lengauer, T., 2002. A hypergraph-based method for unification of existing protein structure- and sequence-families. In Silico Biol. (Gedrukt) 2, 339–349.

Gallivan, J.P., Dougherty, D.A., 1999. Cation-π interactions in structural biology. Proc. Natl. Acad. Sci. U. S. A. 96, 9459–9464.

Gonzalez, M.W., DeVico, A.L., Lewis, G.K., Spouge, J.L., 2015. Conserved molecular signatures in gp120 are associated with the genetic bottleneck during simian immunodeficiency virus (SIV), SIV-human immunodeficiency virus (SHIV), and HIV type 1 (HIV-1) transmission. J. Virol. 89, 3619–3629.

Gracie, J.A., Robertson, S.E., McInnes, I.B., 2003. Interleukin-18. J. Leukoc. Biol. 73, 213–224.

Guex, N., Peitsch, M.C., 1997. SWISS-MODEL and the Swiss-PdbViewer: an environment for comparative protein modeling. Electrophoresis 18, 2714–2723.

Gupta, R., Li, W., Yan, X.J., Barrientos, J., Kolitz, J.E., Allen, S.L., Rai, K., Chiorazzi, N., Mongini, P.K.A., 2019. Mechanism for IL-15-driven B cell chronic lymphocytic leukemia cycling: roles for AKT and STAT5 in modulating cyclin D2 and DNA damage response proteins. J. Immunol. 202, 2924–2944.

Hamasaki, T., Hashiguchi, S., Ito, Y., Kato, Z., Nakanishi, K., Nakashima, T., Sugimura, K., 2005. Human anti–human IL-18 antibody recognizing the IL-18–binding site 3 with IL-18 signaling blocking activity. J. Biochem. 138, 433–442.

Haydarlou, R., Jacobsen, A., Bonzanni, N., Feenstra, K.A., Abeln, S., Heringa, J., 2016. BioASF: a framework for automatically generating executable pathway models specified in BioPAX. Bioinformatics 32, i60–i69.

Henikoff, S., Henikoff, J.G., 1992. Amino acid substitution matrices from protein blocks. Proc. Natl. Acad. Sci. U.S.A. 89, 10915–10919.

Ho, K.C., Hamelberg, D., 2018. Combinatorial coarse-graining of molecular dynamics simulations for detecting relationships between local configurations and overall conformations. J. Chem. Theory Comput. 14, 6026–6034.

Huang, Y.M., Munguia, J., Miao, Y., Nizet, V., McCammon, J.A., 2019. Docking simulation and antibiotic discovery targeting the MlaC protein in Gram-negative bacteria. Chem. Biol. Drug Des. 93, 647–652.

Humphrey, W., Dalke, A., Schulten, K., 1996. VMD: visual molecular dynamics. J. Mol. Graph. 14, 33–38.

Jang, H., Banerjee, A., Marcus, K., Makowski, L., Mattos, C., Gaponenko, V., Nussinov, R., 2019. The structural basis of the farnesylated and methylated KRas4B interaction with calmodulin. Structure 27, 1647–1659 e1644.

Janwa, H., Massey, S.E., Velev, J., Mishra, B., 2019. On the origin of biomolecular networks. Front. Genet. 10.

Jiang, Y., Wang, Y., Pang, W., Chen, L., Sun, H., Liang, Y., Blanzieri, E., 2015. Essential protein identification based on essential protein-protein interaction prediction by Integrated Edge Weights. Methods 83, 51–62.

Jin, Z., Wang, Y., Yu, X.F., Tan, Q.Q., Liang, S.S., Li, T., Zhang, H., Shaw, P.C., Wang, J., Hu, C., 2020. Structure-based virtual screening of influenza virus RNA polymerase inhibitors from natural compounds: molecular dynamics simulation and MM-GBSA calculation. Comput. Biol. Chem. 85, 107241.

Kabat, E.A., 1968. Structural Concepts in Immunology and Immunochemistry. Holt, Rinehart and Winston Inc., New York.

Kato, Z., Jee, J., Shikano, H., Mishima, M., Ohki, I., Ohnishi, H., Li, A., Hashimoto, K., Matsukuma, E., Omoya, K., Yamamoto, Y., Yoneda, T., Hara, T., Kondo, N., Shirakawa, M., 2003. The structure and binding mode of interleukin-18. Nat. Struct. Biol. 10, 966–971.

Kimura, T., Kato, Z., Ohnishi, H., Tochio, H., Shirakawa, M., Kondo, N., 2008. Expression, purification and structural analysis of human IL-18 binding protein: a potent therapeutic molecule for allergy. Allergol. Int. 57, 367–376.

Krumm, B., Meng, X., Li, Y., Xiang, Y., Deng, J., 2008. Structural basis for antagonism of human interleukin 18 by poxvirus interleukin 18-binding protein. Proc. Natl. Acad. Sci. U.S.A. 105, 20711–20715.

Kumar, S., Stecher, G., Tamura, K., 2016. MEGA7: molecular evolutionary genetics analysis version 7.0 for bigger datasets. Mol. Biol. Evol. 33, 1870–1874.

Kwak, Y., Alsaihati, B., Zhang, C., Xu, Y., Cao, S., 2018. The interplay of immune components and ECM in oral cancer. bioRxiv 259622.

Laberge, M., Yonetani, T., 2008. Molecular dynamics simulations of hemoglobin A in different states and bound to DPG: effector-linked perturbation of tertiary conformations and HbA concerted dynamics. Biophys. J. 94, 2737–2751.

Lin, G.N., Corominas, R., Nam, H.J., Urresti, J., Iakoucheva, L.M., 2017. Comprehensive analyses of tissue-specific networks with implications to psychiatric diseases. Methods Mol. Biol. 1613, 371–402.

Lovell, S.C., Davis, I.W., Arendall, W.B., de Bakker 3rd, P.I., Word, J.M., Prisant, M.G., Richardson, J.S., Richardson, D.C., 2003. Structure validation by Calpha geometry: phi,psi and Cbeta deviation. Proteins 50, 437–450.

Mak, T.W., Saunders, M.E., 2006. T cell differentiation and effector function. In: Mak, T.W., Saunders, M.E. (Eds.), The Immune Response. Academic Press, Burlington, pp. 403–432.

Mariethoz, J., Khatib, K., Alocci, D., Campbell, M.P., Karlsson, N.G., Packer, N.H., Mullen, E.H., Lisacek, F., 2016. SugarBindDB, a resource of glycan-mediated host-pathogen interactions. Nucleic Acids Res. 44, D1243–1250.

Moczydlowski, E.G., 2013. The molecular mystique of tetrodotoxin. Toxicon 63, 165–183.

Nakamura, S., Otani, T., Okura, R., Ijiri, Y., Motoda, R., Kurimoto, M., Orita, K., 2000. Expression and responsiveness of human interleukin-18 receptor (IL-18R) on hematopoietic cell lines. Leukemia 14, 1052–1059.

Ohnishi, H., Tochio, H., Kato, Z., Kawamoto, N., Kimura, T., Kubota, K., Yamamoto, T., Funasaka, T., Nakano, H., Wong, R.W., Shirakawa, M., Kondo, N., 2012. TRAM is

involved in IL-18 signaling and functions as a sorting adaptor for MyD88. PLoS One 7, e38423.

Orchard, S., Kerrien, S., Abbani, S., Aranda, B., Bhate, J., Bidwell, S., Bridge, A., Briganti, L., Brinkman, F.S., Cesareni, G., Chatr-aryamontri, A., Chautard, E., Chen, C., Dumousseau, M., Goll, J., Hancock, R.E., Hannick, L.I., Jurisica, I., Khadake, J., Lynn, D.J., Mahadevan, U., Perfetto, L., Raghunath, A., Ricard-Blum, S., Roechert, B., Salwinski, L., Stümpflen, V., Tyers, M., Uetz, P., Xenarios, I., Hermjakob, H., 2012. Protein interaction data curation: the International Molecular Exchange (IMEx) consortium. Nat. Methods 9, 345–350.

OriginLab Corporation, 2016. (version 2016) OriginLab Corporation. Northampton, MA, USA.

Phillips, J., Braun, R., Wang, W., Gumbart, J., Tajkhorshid, E., Villa, E., Chipot, C., Skeel, R., Kale, L., Schulten, K., 2005. Scalable molecular dynamics with NAMD. J. Comput. Chem. 26, 1781–1802.

Průša, J., Cifra, M., 2019. Molecular dynamics simulation of the nanosecond pulsed electric field effect on kinesin nanomotor. Sci. Reports 9, 19721.

Roy, U., 2016a. Structural biology of tumor necrosis factor demonstrated for under-graduate instruction by computer simulation. Biochem. Mol. Biol. Educ. 44, 246–255.

Roy, U., 2016b. Structural characterizations of the fas Receptor and the fas-associated protein with death domain interactions. Protein J. 35, 51–60.

Roy, U., 2017. Structural modeling of tumor necrosis factor: a protein of immunological importance. Biotechnol. Appl. Biochem. 64 (4), 454–463.

Roy, U., 2019a. 3D modeling of tumor necrosis factor receptor and tumor necrosis factor-bound receptor systems. Mol. Inform. 38, e1800011.

Roy, U., 2019b. Structure and function of an inflammatory cytokine, interleukin-2, ana-lyzed using the bioinformatic approach. Protein J. 38 (5), 525–536.

Roy, U., 2020. Structural and molecular analyses of functional epitopes and escape mu-tants in Japanese encephalitis virus envelope protein domain III. Immunol. Res. 68, 81–89.

Roy, U., Luck, L.A., 2007. Molecular modeling of estrogen receptor using molecular op-erating environment. Biochem. Mol. Biol. Educ. 35, 238–243.

Roy, U., Luck, L.A., 2011. Cysteine residues in heavy metal binding proteins: structural insights and comparison with leucine binding protein. JCCE. 5, 771–777.

Roy, U., Chatterjee Debnath, M., Sanyal, K., Das, M.K., Banerjee, S., 2006. Role of pro-tecting groups in the preparation of thiolate complexes of technetium-99 m using cysteine as a model. J. Label. Compd. Radiopharm. 49, 835–847.

Shannon, P., Markiel, A., Ozier, O., Baliga, N.S., Wang, J.T., Ramage, D., Amin, N., Schwikowski, B., Ideker, T., 2003. Cytoscape: a software environment for integrated models of biomolecular interaction networks. Genome Res. 13, 2498–2504.

Sievers, F., Wilm, A., Dineen, D., Gibson, T.J., Karplus, K., Li, W., Lopez, R., McWilliam, H., Remmert, M., Soding, J., Thompson, J., Higgins, D., 2011. Fast, scalable gen-eration of high-quality protein multiple sequence alignments using Clustal Omega. Mol. System Biol. 7, 539.

Taylor, W.R., Stoye, J.P., Taylor, I.A., 2017. A comparative analysis of the foamy and

ortho virus capsid structures reveals an ancient domain duplication. BMC Struct. Biol. 17, 3.

Tsutsumi, N., Kimura, T., Arita, K., Ariyoshi, M., Ohnishi, H., Yamamoto, T., Zuo, X., Maenaka, K., Park, E.Y., Kondo, N., Shirakawa, M., Tochio, H., Kato, Z., 2014. The structural basis for receptor recognition of human interleukin-18. Nature Commun. 5, 5340.

Tsutsumi, N., Yokota, A., Kimura, T., Kato, Z., Fukao, T., Shirakawa, M., Ohnishi, H., Tochio, H., 2019. An innate interaction between IL-18 and the propeptide that in-activates its precursor form. Sci. Rep. Ist. Super. Sanita 9, 6160.

VanSchouwen, B.M., Gordon, H.L., Rothstein, S.M., Komeiji, Y., Fukuzawa, K., Tanaka, S., 2008. Water-mediated interactions in the CRP-cAMP-DNA complex: does water mediate sequence-specific binding at the DNA primary-kink site? Comput. Biol. Chem. 32, 149–158.

Vogt, B., Hofmann, K., 2012. Bioinformatical detection of recognition factors for ubiquitin and SUMO. Methods Mol. Biol. 832, 249–261.

Voit, E.O., 2014. Mesoscopic modeling as a starting point for computational analyses of cystic fibrosis as a systemic disease. Biochim. Biophys. Acta 1844, 258–270.

Wang, X., Yu, B., Ma, A., Chen, C., Liu, B., Ma, Q., 2018. Protein–protein interaction sites prediction by ensemble random forests with synthetic minority oversampling tech-nique. Bioinformatics 35, 2395–2402.

Weako, J., Uba, A.I., Keskin, Ö., Gürsoy, A., Yelekçi, K., 2020. Identification of potential inhibitors of human methionine aminopeptidase (type II) for cancer therapy: struc-ture-based virtual screening, ADMET prediction and molecular dynamics studies. Comput. Biol. Chem., 107244.

Xiao, H., Bartoszek, K., Lio', P., 2018. Multi–omic analysis of signalling factors in in-flammatory comorbidities. BMC Bioinformatics 19, 439.

Yamamoto, Y., Kato, Z., Matsukuma, E., Li, A., Omoya, K., Hashimoto, K., Ohnishi, H., Kondo, N., 2004. Generation of highly stable IL-18 based on a ligand-receptor com-plex structure. Biochem. Biophys. Res. Commun. 317, 181–186.

Yao, X.Q., Momin, M., Hamelberg, D., 2019. Establishing a framework of using residue-residue interactions in protein difference network analysis. J. Chem. Inf. Model. 59, 3222–3228.

Zalinger, Z.B., Elliott, R., Weiss, S.R., 2017. Role of the inflammasome-related cytokines Il-1 and Il-18 during infection with murine coronavirus. J. Neurovirol. 23, 845–854.

Zamiri, B., Reddy, K., Macgregor, R.B., Pearson Jr., C.E., 2014. TMPyP4 porphyrin dis-torts RNA G-quadruplex structures of the disease-associated r(GGGGCC)n repeat of the C9orf72 gene and blocks interaction of RNA-binding proteins. J. Biol. Chem. 289, 4653–4659.

Zhang, X., Liu, P., Zhang, C., Chiewchengchol, D., Zhao, F., Yu, H., Li, J., Kambara, H., Luo, K.Y., Venkataraman, A., Zhou, Z., Zhou, W., Zhu, H., Zhao, L., Sakai, J., Chen, Y., Ho, Y.-S., Bajrami, B., Xu, B., Silberstein, L.E., Cheng, T., Xu, Y., Ke, Y., Luo, H.R., 2017. Positive regulation of interleukin-1β bioactivity by physiological ROS-medi-ated cysteine S-glutathionylation. Cell Rep. 20, 224–235.